THE EFFECT OF NICKEL CONTENT, SINTERING TEMPERATURE AND DENSITY ON THE PROPERTIES OF A WARM COMPACTED 0.85 w/o MOLYBDENUM PREALLOY

Amie H. Graham, Tina M. Cimino, Arthur J. Rawlings, Howard G. Rutz
Hoeganaes Corporation, Riverton, NJ 08077

Presented at PM² TEC '97
International Conference on Powder Metallurgy & Particulate Materials
June 29- July 2, 1997 Chicago, IL USA

ABSTRACT

The combination of molybdenum prealloyed steel powders and admixed nickel provides sintered steels that are used in structural parts requiring strength, wear resistance, and impact toughness. The properties of these materials, like all P/M steels, are dependent on density, microstructure and composition.

This work discusses the effect of admixed nickel content, sintering temperature, and density on the properties of a 0.85 w/o molybdenum prealloy. Samples were prepared with 0, 2, 4 and 6 w/o nickel additions. The materials were warm compacted at 30, 40, 45, and 50 tsi (415, 550, 620 and 690 MPa) and sintered at 1900°F, 2100°F and 2300°F (1040°C, 1150°C, and 1260°C). Mechanical properties were determined and related to the density, microstructure, and composition.

INTRODUCTION

The use of 0.85 w/o molybdenum prealloyed powder has resulted in several distinct benefits to P/M parts producers [1-3]. This material, used in combination with a variety of premix additives, provides excellent strength in the as-sintered, sinter-hardened as well as quenched and tempered condition, and also can be induction hardened. When combined with nickel admix additions, these materials provide excellent dimensional stability with little variation in dimensional change across a wide range of density levels. This helps to limit distortion in complex shapes with large density gradients and thus provides better dimensional tolerances. These material combinations also provide good dimensional stability for heat treated parts.

The prealloyed molybdenum, while providing excellent hardenability, does not strengthen ferrite to the degree of prealloyed nickel additions and thus provides excellent compressibility. Green density levels on the order of non-alloyed iron powders are readily achievable in normal compaction. The material is an excellent candidate for the ANCORDENSE® [4-6] process, where high density levels achievable with the warm compaction process can be combined with the high strength levels of the alloy system to provide high performance P/M components.

This paper will review several aspects of process variables for a 0.85 w/o molybdenum prealloy base material combined with various levels of admixed nickel. In addition to evaluating the

effect of nickel content, sintering will be conducted across a wide range of temperatures. The use of warm compaction will be utilized to evaluate performance at high density levels. The evolution of the microstructure with varying nickel content, sintering temperature and density

Ancorsteel® 85 HP	0.85	--	0.50
	0.85	2.00	0.50
	0.85	4.00	0.50
	0.85	6.00	0.50

will be related to mechanical properties.

EXPERIMENTAL PROCEDURE

Materials

In order to evaluate the effect of density, microstructure and composition on mechanical properties, premixes were prepared using ANCORDENSE processing. The premix

Green Strength	30/*415*	1900/*1040°C*
	40/*550*	2100/*1150°C*
Tensile	45/*620*	2300/*1260°C*
	50/*690*	

compositions are shown in Table I. In all cases, 0.60 w/o of the ANCORDENSE lubricant was added to the binder treated premixes. The nickel utilized in these premixes was Inco 123, and the graphite was Asbury 3203 SCR HS.

Table I: Premix Compositions

Test Specimen Preparation

Test specimens were compacted utilizing the ANCORDENSE process with the powder and tooling heated to 290°F/145°C. Compaction and processing variables are listed in Table I1:

Table I1: Processing Variables

The transverse rupture strength (TRS) and tensile bars were at the sintering temperature for 30 minutes with the furnace atmosphere set to 75 v/o N/25 v/o H_2.

Testing

All samples were prepared and tested according to the appropriate MPIF standard [7]. Green density, green strength, and green expansion were determined from the average of five compacted green strength bars with a nominal size of 0.5 inches x 0.5 inches x 1.25 inches (12.7 mm x 12.7 mm x 31.75 mm). Green strength was determined via a three point bend test on a Tinius Olsen testing machine with a 5,000 lb. load cell.

TRS bars of a nominal size of 0.25 inches x 0.5 inches x 1.25 inches (6.35 mm x 12.7 mm x 31.75 mm) were compacted, sintered, and utilized to determine sintered density, sintered dimensional change (from die), apparent hardness, and modulus of rupture (TRS). Five samples from each mix were prepared under each condition. The specimens were broken on a Tinius Olsen testing machine fitted with a 10,000 lb. load cell. Apparent hardness measurements were performed using a Rockwell Hardness Tester. The testing was performed on the Rockwell B or C scale depending on the apparent hardness of the material.

Tensile testing was performed on dogbone specimens on a 60,000 pound Tinius Olsen universal testing machine at a crosshead speed of 0.1 inches/minute. Elongation values were determined utilizing an extensometer with a range of 0 to 20%. The extensometer was left on each test specimen until failure.

Metallography

The tensile bars were sectioned in the grip area and prepared for metallographic analysis. The microstructure was evaluated following a 2% nital/4% picral etch, and photomicrographs were prepared.

RESULTS & DISCUSSION

Green Properties

The green density, green expansion, and green strength results for each compaction pressure for the tested mixes are presented in Table II1.

As expected, green density increases with increased compaction pressure (Figure 1). The addition of nickel has little effect on the green density with the exception of the results at 50 tsi (690 MPa). At this compaction pressure, the green density increases with increasing nickel content. In evaluating the pore free density values calculated for each of the mixes, increasing the nickel content by increments of 2 w/o results in increases of the pore free density of on average, 0.017 g/cm$^{a\cdot}$ At 50 tsi (690 MPa), each material reaches between 97.8 and 97.9% of the calculated pore free density. This indicates that the materials have essentially reached the maximum green density possible, and compaction beyond this pressure will generally not result in further increases in green density.

At Low densities, all of the nickel mixes have similar green expansion; the mix with no added nickel has slightly lower green expansion (Figure 2). At higher densities, the mixes tend to spread out. The 2 w/o nickel mix has the most green expansion followed by the 4 w/o nickel mix and the 6 w/o nickel mix, respectively. However, the mix with no nickel indicates the least green expansion.

The material with no nickel has the highest green strength at approximately 3,700 psi (26 MPa) and does not change significantly with increasing density (Figure 3). The 2, 4, and 6 w/o nickel mixes all have similar green strengths, around 3,200 psi (22 MPa). With these materials, the green strength increases only slightly with increased density.

It is apparent that green properties are not drastically affected by the addition of nickel. The green density is relatively unchanged but shows the effect of nickel on pore free density and the resulting green density at higher compaction pressures. The addition of nickel increases the green expansion slightly compared with the mix with no nickel addition, but increased amounts of nickel decrease this difference in green expansion. The green strength is fairly consistent with each mix.

At 1900°F, 2100°F, and 2300°F (1040°C, 1150°C, and 1260°C), as expected, the sintered density increases with compaction pressure. As the nickel content increases, the sintered density also increases for a given sintering temperature. The effect of nickel content is most obvious at the highest sintering temperature and least at the lowest sintering temperature (Figures 4 and 5). When comparing each individual mix, as the sintering temperature increases, the density also increases. In the mix with no nickel addition, there was only a slight increase in density seen with increased sintering temperature. However, as the nickel content is increased, the effect of increasing temperature becomes more pronounced.

At all temperatures, the amount of shrinkage increased with increasing nickel content. Dimensional change was fairly consistent at all densities for any given mix, but did increase slightly with increased density. As the nickel content was increased, the amount of difference in dimensional change for a given density increased slightly. When looking at the individual mixes, the amount of shrinkage increased with increasing sintering temperature. The effect of nickel content on dimensional change at 2100°F (1150°C) is illustrated in Figure 6. Figure 7 shows the relationship between dimensional change and sintering temperature for the FLN2-4405 material. These relationships hold true for the other sintering temperatures and nickel contents.

In general, TRS increases with increasing nickel content and density. In the 0 w/o nickel mix, the TRS values increase with increased temperature, though the 2100°F (1150°C) and 2300°F (1260°C) values remain close together. In the 2 w/o nickel sample, TRS values increase with increased temperature, though the 2100°F (1150°C) and 2300°F (1260°C) values are even closer together than the 0 w/o nickel sample. The values start to overlap at high densities. In the 4 w/o nickel sample, TRS increases from 1900°F (1040°C) to 2100°F (1150°C), but with increased temperature to 2300°F (1260°C), no improvement in TRS is seen. At 6 w/o nickel, TRS increases with temperature and density, but at all temperatures, when the samples are pressed at a pressure higher than 45 tsi (620 MPa), the TRS decreases. These trends can be viewed in Figures 8 and 9.

At all temperatures, apparent hardness increases with increased nickel content. At 0 w/o nickel, an increase in hardness is seen as the sintering temperature is increased from 1900°F (1040°C) to 2100°F (1150°C). Increasing the sintering temperature to 2300°F (1260°C) provides no improvement in surface hardness for this mix. At 2 w/o nickel, hardness remains relatively constant at all temperatures but increases with density. At 4 w/o nickel, hardness increases from 1900°F (1040°C) to 2100 °F, but no improvement is seen in hardness when the sintering temperature is increased to 2300°F (1260°C). At 6 w/o nickel, hardness increases with sintering temperature. These trends can be seen in Figures 10 and 11.

The TRS and apparent hardness data both follow the same trends. At 0, 2, and 4 w/o nickel, no improvement is seen on sintering at 2300°F (1260°C) versus the lower temperatures. On the other hand, the 6 w/o nickel sample experiences an increase in both TRS and hardness on sintering at 2300°F (1260°C).

Tensile Properties

In general, ultimate tensile strength (UTS) increases with increasing nickel content and density. In the 0 w/o nickel samples, the UTS values increase with increased temperature. In the 2 and 4 w/o nickel samples, UTS increases from 1900°F (1040°C) to 2100°F (1150°C), but when the sintering temperature is increased to 2300°F (1260°C), no further improvement in UTS is realized. At 6 w/o nickel, UTS increases with temperature and density, but at 2300°F (1260°C), when the samples are compacted at a pressure higher than 40 tsi (550 MPa), the UTS decreases. Figures 12 and 13 depict these trends graphically.

In general, the 0.2% offset yield strength tends to increase with increased nickel content. Yield strength increases only slightly with increased density. At 1900°F (1040°C), yield strength increases with nickel content from 0 to 2 w/o and 2 to 4 w/o, but upon increasing the nickel content to 6 w/o, no increase in yield strength is seen. At 2100°F (1150°C) and 2300°F (1260°C), yield strength increases with increased nickel content. At 0 w/o nickel, yield strength increases only slightly with sintering temperature. At 2 w/o, the same trend is found, but the values are slightly higher than 0 w/o nickel. At 4 w/o nickel, a spread is seen in the yield strength values; as the temperature increases, the yield strength increases. At 6 w/o nickel, an even larger yield strength increase is realized with increased sintering temperature.

In general, at 1900°F (1040°C) and 2100°F (1150°C), each of the mixes exhibit similar elongation values. At 2300°F (1260°C), the elongation values spread out and it becomes evident that elongation values decrease as nickel content increases. For the 0 and 2 w/o nickel samples, elongation increases as sintering temperature increases. At 4 w/o nickel, elongation increases from 1900°F (1040°C) to 2100°F (1150°C), but sees no improvement upon sintering at 2300°F (1260°C). With the 6 w/o nickel material, elongation increases from 1900°F (1040°C) to 2100°F (1150°C), but sees a decrease upon sintering at 2300°F (1260°C). These relationships are depicted in Figures 14, 15, and 16.

Microstructure Analysis

The mechanical properties of the materials can be explained through the analysis of their respective microstructures. Photomicrographs, taken at an original magnification of 500X, of the different materials compacted at 40 tsi (550 MPa) and sintered at each of the three sintering temperatures are shown in Figures 17 through 28. In all cases, the degree of sinter, reflected in the amount of interparticle bonding in the early stage of sintering and the rounding and coalescence of the porosity, changes significantly with sintering temperature and nickel content. At higher sintering temperatures, pore rounding and pore coalescence takes place, particularly in the materials with admixed nickel. These phenomena are manifested as densification through shrinkage during sintering. As mentioned above, as the nickel content increased or the sintering temperature was elevated, the amount of shrinkage also increased. Although the pore structure may be considered a major component of the microstructure, in the following discussion, changes in pore structure and interparticle bonding will be considered separately from the more traditional metallurgical aspects of microstructure (e.g. constituents such as pearlite and martensite).

For the 0 w/o nickel material, (Figures 17, 18, and 19), the microstructures produced at 1900°F (1040°C), 2100°F (1150°C), and 2300°F (1260°C) are very similar and consist of coarse divorced pearlite. At 1900°F (1040°C), the sample exhibits a poor degree of sinter. As the sintering

temperature increases to 2100°F (1150°C) (Figure 18), the grain size increases slightly and the sinter is improved. By increasing the temperature to 2300°F (1260°C), other than some pore refinement, no significant change is noted (Figure 19).

The sample of the mix with 2 w/o nickel (Figure 20), sintered at 1900°F (1040°C), exhibits a structure that still consists mainly of divorced pearlite. However, the spacing is much finer than found in the samples without nickel additions. There are also regions of very fine, unresolved pearlite and small nickel rich regions. At this temperature, the sample exhibits a poor degree of sinter but appears somewhat improved over the 0 w/o nickel sample sintered at the same temperature. At 2100°F (1150°C) (Figure 21), the degree of sinter improves and the nickel diffusion is more complete. Some transformation to martensite is seen as the concentration of nickel is decreased. The pearlite structure remains the same with fine divorced pearlite and unresolved pearlite. At 2300°F (1260°C) (Figure 22), almost all of the nickel rich regions transform into martensite. There also appears to be somewhat less unresolved pearlite, and the spacing of the divorced pearlite becomes slightly finer although these changes are fairly minor.

At 4 w/o nickel (Figures 23, 24, and 25), very similar microstructural changes to the 2 w/o nickel sample are seen. At 1900°F (1040°C), the structure consists mainly of divorced pearlite, very fine unresolved pearlite and nickel rich regions that are larger in size and concentration than found in the 2 w/o nickel sample. This sample also exhibits a poor degree of sinter but perhaps not as poor as seen in the 0 w/o nickel material. At 2100°F (1150°C), the sinter and the nickel diffusion is better and some transformation to martensite is seen as the concentration of nickel is decreased. The pearlite structure is still a combination of divorced pearlite with fine unresolved pearlite clusters. At 2300°F (1260°C), most of the nickel rich regions transform into martensite, with the amount of martensite greater than for the 2 w/o nickel sample sintered at the same temperature.

The microstructures of the 6 w/o nickel samples (Figures 26, 27, and 28) are different than the other nickel bearing materials. At 1900°F (1040°C), the sample has a significantly higher level of nickel rich areas and unresolved pearlite nearly equally split in volume with the divorced pearlite areas. The degree of sinter is difficult to see in the etched photomicrographs but is not as poor as the other samples sintered at the same temperature. Some diffusion has taken place, but there is little transformation of the nickel rich areas into martensite. At 2100°F (1150°C), more nickel diffusion is apparent and there is significant martensitic transformation, with about half of the nickel rich areas consisting of martensite. There are also areas of very fine divorced pearlite and unresolved pearlite. At 2300°F (1260°C), more complete nickel diffusion has produced a near complete martensite transformation in the nickel rich areas with some areas of fine divorced pearlite and unresolved pearlite.

The analysis of the evolution of the microstructures through the use of various nickel contents and sintering temperatures can be utilized to explain the mechanical properties reported earlier. In the case of the 0 w/o nickel mix, the properties increase significantly as the sintering temperature is increased from 1900°F (1040°C) to 2100°F (1150°C). This increase in properties is due primarily to the improvement in particle sintering, as the microstructural constituents do not change significantly. As the temperature is increased to 2300°F (1260°C), the increase in performance is less, with the greatest changes occurring in ductility and UTS improvements. Again, the microstructure does not change significantly, and the increase in ductility of the

material can be related more to the change in the sintering. Interestingly, there is nearly no change in apparent hardness values for a given density level across all three sintering temperatures, indicating that microstructure, rather than the degree of sinter, is the major factor affecting this parameter.

In the 2 w/o nickel material, the apparent hardness, TRS, and UTS increase as the sintering temperature is raised from 1900°F (1040°C) to 2100°F (1150°C). This again appears to be due to the improvement in the degree of sinter rather than significant changes in the microstructural constituents. No significant change in hardness or strength is seen by increasing the temperature to 2300°F (1260°C), but the elongation values increase significantly. The most significant change in the microstructure at this temperature is the transformation of the nickel rich areas to martensite. This appears to have little effect on the overall strength of the material and no effect on the ductility. The material sintered at 2300°F (1260°C) appears to have improved ductility through pore refinement and interparticle bonding.

The 4 w/o nickel material generally follows the same trends as the sintering temperature is increased from 1900°F (1040°C) to 2100°F (1150°C), and the strength and elongation values increase significantly. Most of this increase can be attributed to the improvement in the degree of sinter at the higher temperature. With this material there is a slightly greater increase in apparent hardness for a given density than was seen in the previous two materials. This indicates that enough nickel rich area has been transformed to martensite to make a measurable difference in the hardness level. As the sintering temperature is raised to 2300°F (1260°C), the strength values increase. The elongation values also increase but at a much lower rate than is found for this temperature increase for the O and 2 w/o nickel materials. These results indicate that there is enough martensite in the microstructure to increase strength while decreasing ductility enough to offset the gain expected from sintering improvements.

The 6 w/o nickel mix indicates the most significant changes in microstructure and properties with increasing sintering temperature. The apparent hardness, yield strength and TRS value all increase as the sintering temperature increases. The significant amount of the increase can be attributed largely to the increase in martensite in the microstructure. The effect of sintering improvements, although important, are overshadowed by the microstructural change. Interestingly, when the sintering temperature is increased from 2100°F (1150°C) to 2300°F (1260°C), the UTS remains constant while the elongation actually decreases. Both of these results can be attributed to the lowering of ductility, as the material becomes more martensitic. The results are an indication that the test specimens may be breaking prematurely due to the brittle nature of the material, so the true ultimate load is not reached. This would result in a lessening of the UTS and elongation values. This result may be expected given that a dogbone tensile test specimen was used. This geometry, with square corners in the gauge length, would certainly tend to fail sooner in a brittle material. The use of a machined round bar for testing this harder material would yield more reliable data.

At each sintering temperature, apparent hardness, TRS, and UTS increase with increased nickel content. Two effects contribute to this result. As the nickel content is increased, the degree of sinter appears to improve contributing to increased performance levels. In particular, at 1900°F (1040°C), the amount of interparticle bonding is improved due to increased nickel content by the formation of well sintered nickel rich areas. At the higher sintering temperatures, the nickel

appears to contribute to pore refinement. The nickel also plays an important role in defining the microstructural constituents. The increased nickel content plays a more important role as the sintering temperature is increased. The diffusion of the nickel and eventual transformation of nickel rich areas into martensite has a potent effect on increasing hardness and strength while decreasing ductility.

CONCLUSIONS

1. The effect of density, sintering temperature and admixed nickel content on a warm compacted 0.85 w/o molybdenum prealloy was evaluated. The following can be concluded from the testing:

2. The use of warm compaction provided green density levels of about 7.0 g/cm^3 at 30 tsi (415 MPa) and 7.3 g/cm^3 at 50 tsi (690 MPa). At 50 tsi (690 MPa), all four mixes in the study attained approximately 97.8% of the calculated pore free density. The density level at the highest compaction pressure was related to the nickel content, with higher nickel contents providing slightly higher green density values. As a result of warm compaction, green strength values were in the range of 3000 to 4700 psi (21 to 33 MPa). This is a 50% to 100% improvement over conventional compaction [6].

3. As the sintering temperature increased, strength and apparent hardness values increased. This effect was more pronounced with higher nickel contents. This effect was related to two microstructural changes in the materials. Increased sintering temperature resulted in a better degree of sinter and increased pore refinement. Elevating the sintering temperature also resulted in more complete nickel diffusion. This provides the ability to transform additional material to martensite, increasing strength and apparent hardness.

4. Increasing the nickel content for a given sintering temperature resulted in increased shrinkage and sintered density while improving strength. Elongation values were affected by several factors. At the lower nickel contents and sintering temperature, the presence of nickel appears to aid in sintering and pore refinement, and it results in larger elongation values. As the nickel content and sintering temperature are increased, the formation of martensite reduces the ductility of the material faster than the improvement resulting from sintering. It was postulated that at the highest nickel content and sintering temperature, the test specimen geometry may have produced even greater reductions in the measured elongation and UTS values.

ACKNOWLEDGMENTS

The authors wish to thank Ron Fitzpatrick, Craig Gamble, Steve Kolwicz and Jerry Golin for their assistance in preparing, testing and analyzing the samples. The authors are particularly grateful to Tom Murphy for his assistance in interpreting the microstructures. We would also like to thank Shirley Tworzydlo for her assistance in the preparation of the manuscript.

REFERENCES

1. Causton, R.J., James, W.B., Fulmer, J.J., "Performance Characteristics of a New Sinter-Hardening Low-Alloy Steel", *Advances in Powder Metallurgy - 1991,* Vol. 5, p. 91, Metal Powder Industries Federation, Princeton, NJ.

2. Hamill, J.A., Jr., Causton, R.J., Shah, S., "High Performance Ferrous P/M Materials Utilizing High Temperature Sintering", *Advances in Powder Metallurgy & Particulate Materials -1992,* Vol. 5, p. 193, Metal Powder Industries Federation, Princeton, NJ.

3. Causton, R.J., Fulmer, J.J., "Sinter-Hardening Low-Alloy Steels", *Advances in Powder Metallurgy & Particulate Materials - 1992,* VoL 5, p. 17, Metal Powder Industries Federation, Princeton, NJ.

4. Rutz, H.G., Luk, S.H., "Method of Making a Sintered Metal Component", United States Patent No. 5,154,881.

5. Luk, S.H., "Metal Powder Compositions Containing Binder Agents for Elevated Temperature Compaction", United States Patent No. 5,368,630-Additional Patents Pending.

6. Rutz, H.G., Hanejko, F.G., "High Density Processing of High Performance Ferrous Materials", *Advances in Powder Metallurgy & Particulate Materials - 1994,* Vol. 5, p. 117-133, Metal Powder Industries Federation, Princeton, NJ.

7. "Standard Test Methods for Metal Powders and Powder Metallurgy Products", Metal Powder Industries Federation, Princeton, NJ, 1996.

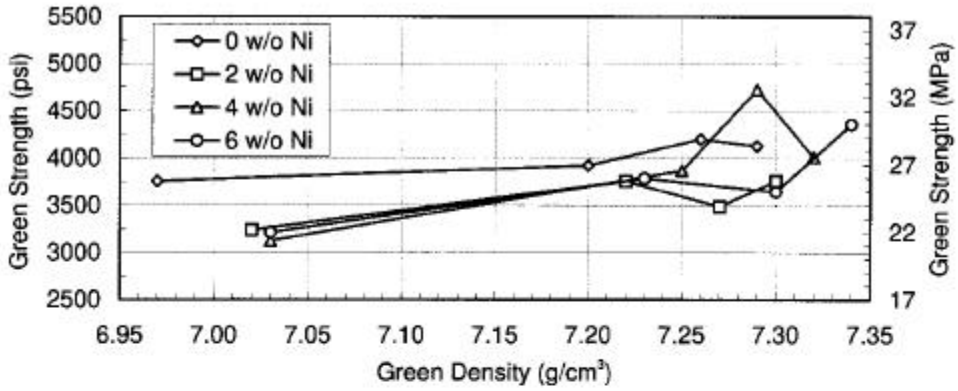

Figure 3: Green Strength as a Function of Green Density for the Materials Tested

Sintered Properties

The sintered properties of the four mixes are represented in Tables IV, V, and VI.

Table IV: Sintered Properties at 1900°F/*1040°C*

dil. (wt%)	Comp. Pressure (psi/MPa)	Sintered Density (g/cm³)	D.C. (%)	TRS (psi x 10³/MPa)	Hard. (HRB)	UTS (psi x 10³/MPa)	YS (psi x 10³/MPa)	Elong. (%)
0	30/*415*	6.95	+0.16	113.3/*781*	70	64.0/*411*	53.6/*370*	1.3
0	40/*550*	7.15	+0.22	124.5/*858*	78	68.3/*471*	56.9/*392*	1.4
0	45/*620*	7.21	+0.25	116.3/*802*	79	67.8/*467*	58.0/*400*	1.4
0	50/*690*	7.24	+0.25	132.0/*910*	82	66.4/*458*	57.5/*396*	1.1
2	30/*415*	7.01	+0.07	139.1/*959*	83	76.1/*525*	62.5/*431*	1.2
2	40/*550*	7.21	+0.14	161.4/*1113*	90	81.5/*562*	67.7/*468*	1.1
2	45/*620*	7.27	+0.15	164.8/*1136*	90	87.1/*601*	70.4/*485*	1.4
2	50/*690*	7.31	+0.15	168.9/*1165*	92	95.0/*655*	72.8/*502*	1.4
4	30/*415*	7.03	+0.02	169.1/*1166*	91	85.0/*586*	66.1/*456*	1.1
4	40/*550*	7.24	+0.05	191.8/*1322*	96	93.6/*645*	72.7/*501*	1.3
4	45/*620*	7.30	+0.10	196.8/*1357*	95	94.5/*652*	74.1/*511*	1.3
4	50/*690*	7.34	+0.12	204.5/*1410*	97	99.5/*686*	75.6/*521*	1.4
6	30/*415*	7.06	-0.06	174.4/*1202*	93	89.6/*618*	66.3/*457*	1.4
6	40/*550*	7.27	-0.01	212.2/*1463*	98	102.0/*703*	73.0/*503*	1.7
6	45/*620*	7.31	+0.05	216.0/*1489*	19 HRC	103.1/*711*	75.1/*518*	1.6
6	50/*690*	7.36	+0.04	201.3/*1388*	19 HRC	108.7/*749*	77.2/*532*	1.8

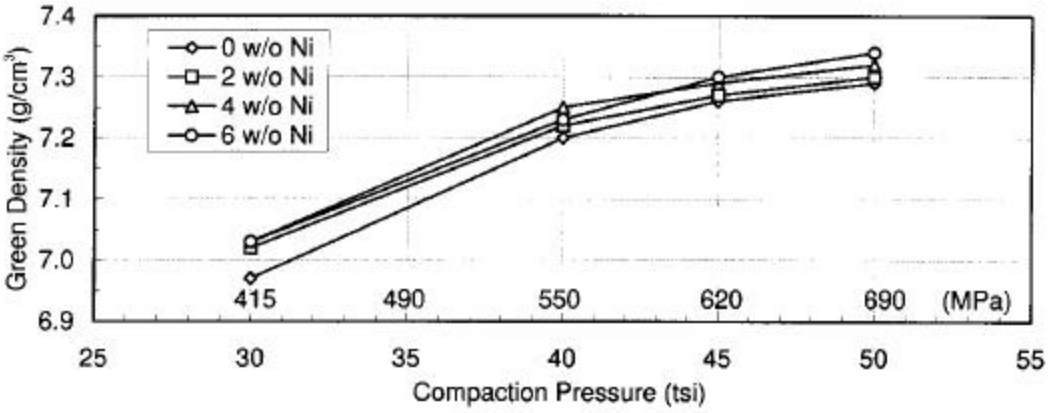

Figure 1: Green Density of Tested Materials as a Result of Compaction Pressure

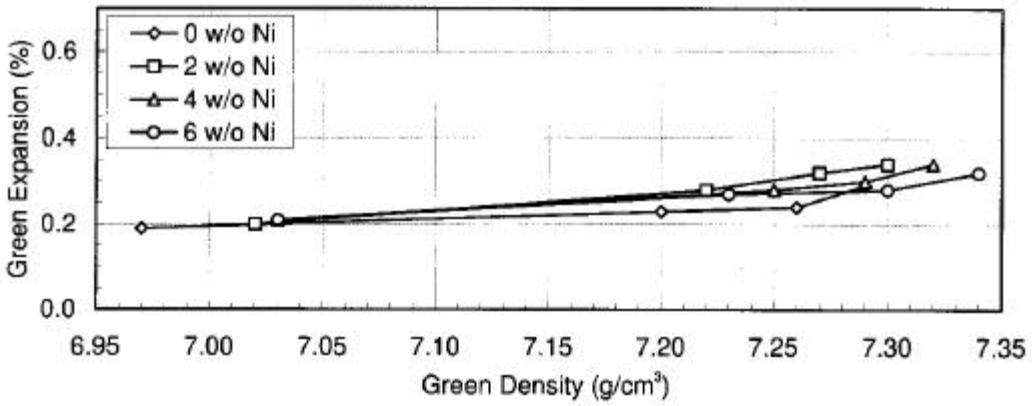

Figure 2: Green Expansion as a Function of Green Density for the Materials Tested

Table V: Sintered Properties at 2100°F/*1150°C*

Ni (w/o)	Comp. Pressure (tsi/*MPa*)	Sintered Density (g/cm³)	D. C. (%)	TRS (psi x 10³/ *MPa*)	Hard. (HRB)	UTS (psi x 10³/ *MPa*)	YS (psi x 10³/ *MPa*)	Elong. (%)
0	30/*415*	6.95	+0.11	132.9/*916*	75	67.0/*462*	53.9/*372*	1.8
0	40/*550*	7.17	+0.16	159.6/*1100*	82	75.6/*521*	59.5/*411*	2.4
0	45/*620*	7.23	+0.16	168.0/*1158*	83	77.4/*534*	60.6/*418*	2.5
0	50/*690*	7.27	+0.15	170.5/*1176*	85	79.4/*547*	61.0/*421*	2.9
2	30/*415*	7.04	-0.09	160.8/*1109*	84	83.3/*574*	63.0/*435*	1.7
2	40/*550*	7.25	-0.05	191.4/*1320*	90	92.7/*639*	68.9/*475*	2.1
2	45/*620*	7.31	-0.03	200.4/*1382*	92	97.4/*672*	72.0/*497*	2.4
2	50/*690*	7.35	-0.01	208.6/*1438*	94	102.4/*706*	74.6/*515*	2.7
4	30/*415*	7.08	-0.21	203.7/*1404*	96	108.4/*747*	74.9/*517*	2.0
4	40/*550*	7.27	-0.13	238.6/*1645*	98	117.9/*813*	80.0/*552*	2.2
4	45/*620*	7.34	-0.13	253.9/*1751*	21 HRC	122.6/*845*	85.7/*591*	2.5
4	50/*690*	7.37	-0.11	266.2/*1835*	23 HRC	128.4/*886*	86.5/*597*	2.6
6	30/*415*	7.12	-0.37	237.8/*1640*	25 HRC	123.3/*851*	81.1/*560*	1.8
6	40/*550*	7.31	-0.27	268.4/*1851*	28 HRC	138.1/*953*	83.7/*578*	2.3
6	45/*620*	7.37	-0.22	297.8/*2053*	29 HRC	144.6/*998*	83.4/*575*	2.5
6	50/*690*	7.41	-0.19	293.8/*2026*	31 HRC	151.5/*1045*	84.0/*580*	2.7

Table VI: Sintered Properties at 2300°F/*1260°C*

Ni (w/o)	Comp. Pressure (tsi/*MPa*)	Sintered Density (g/cm³)	D. C. (%)	TRS (psi x 10³/ *MPa*)	Hard. (HRB)	UTS (psi x 10³/ *MPa*)	YS (psi x 10³/ *MPa*)	Elong. (%)
0	30/*415*	6.98	-0.06	147.4/*1017*	76	73.0/*504*	55.6/*384*	2.4
0	40/*550*	7.20	+0.04	173.7/*1199*	83	83.3/*575*	59.9/*413*	3.6
0	45/*620*	7.26	+0.03	180.8/*1248*	85	85.3/*589*	61.5/*424*	3.9
0	50/*690*	7.30	+0.08	190.0/*1311*	86	85.9/*593*	61.9/*427*	4.1
2	30/*415*	7.08	-0.31	175.6/*1212*	85	85.7/*591*	65.2/*450*	2.2
2	40/*550*	7.29	-0.24	203.4/*1403*	90	96.6/*667*	69.0/*476*	3.4
2	45/*620*	7.35	-0.21	208.4/*1438*	93	100.9/*696*	71.6/*494*	3.7
2	50/*690*	7.38	-0.18	217.9/*1504*	94	104.3/*720*	74.3/*513*	4.5
4	30/*415*	7.12	-0.47	214.6/*1481*	96	111.9/*772*	83.9/*579*	1.8
4	40/*550*	7.32	-0.35	245.4/*1693*	22 HRC	125.9/*869*	85.1/*587*	2.4
4	45/*620*	7.38	-0.32	265.3/*1831*	23 HRC	128.8/*889*	90.8/*626*	2.4
4	50/*690*	7.42	-0.27	271.6/*1874*	24 HRC	136.2/*940*	92.4/*637*	2.8
6	30/*415*	7.17	-0.58	276.1/*1905*	31 HRC	148.4/*1024*	95.3/*657*	1.7
6	40/*550*	7.35	-0.49	306.6/*2115*	34 HRC	159.6/*1101*	103.2/*712*	2.1
6	45/*620*	7.40	-0.41	319.0/*2201*	36 HRC	152.8/*1054*	102.6/*708*	1.9
6	50/*690*	7.44	-0.35	292.0/*2015*	35 HRC	150.6/*1039*	101.6/*701*	1.7

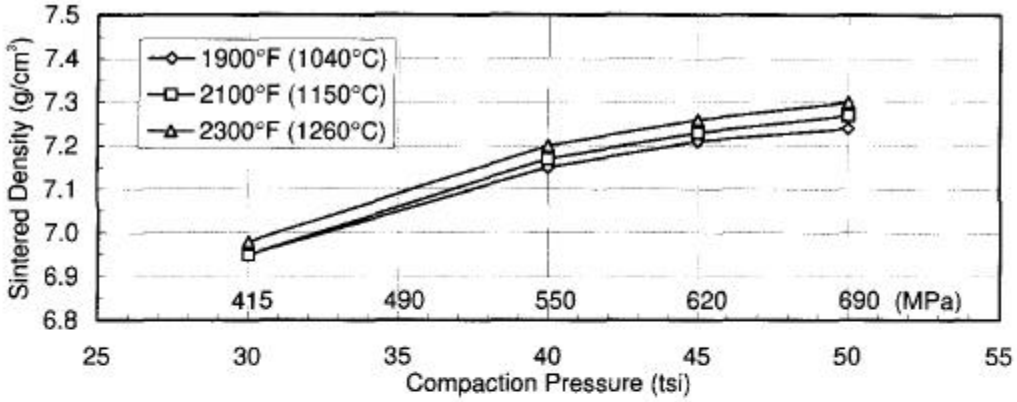

Figure 4: **Sintered Density of FL-4405 as a Result of Compaction Pressure and Sintering Temperature**

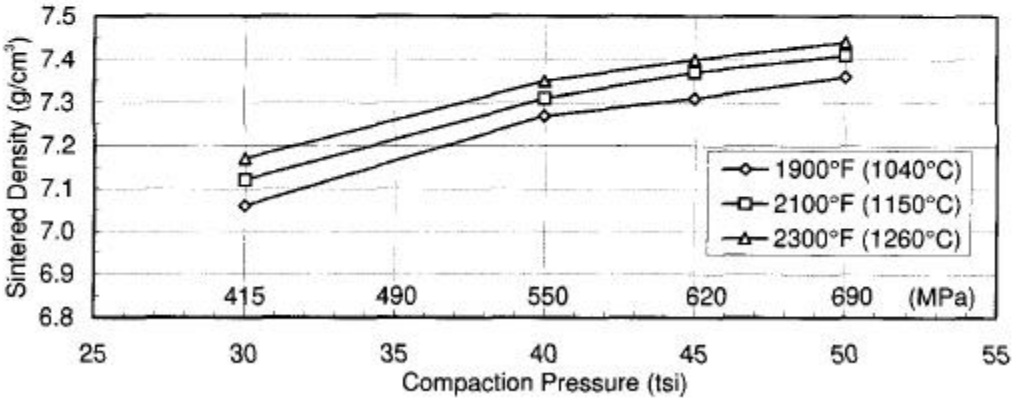

Figure 5: **Sintered Density of FLN6-4405 as a Result of Compaction Pressure and Sintering Temperature**

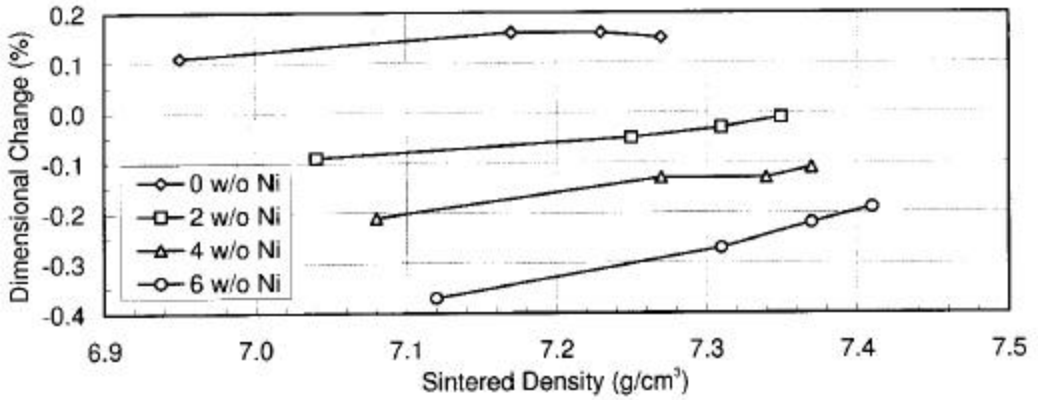

Figure 6: **Dimensional Change as a Function of Sintered Density and Nickel Content at 2100°F (1150°C)**

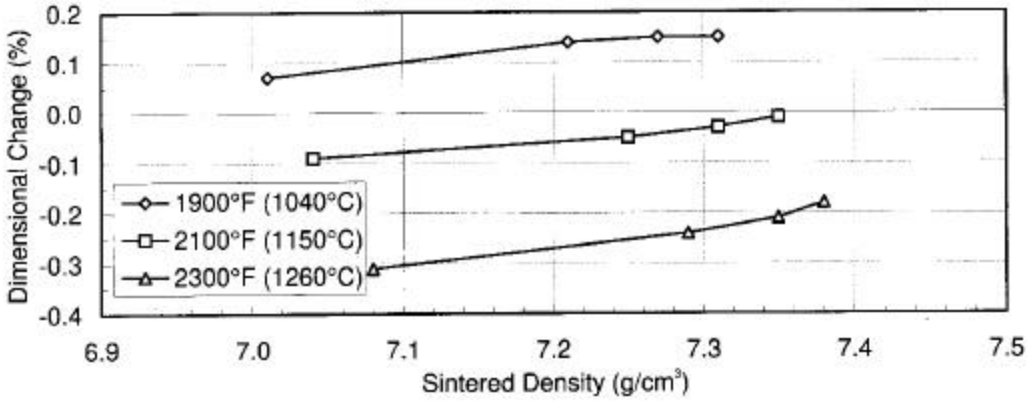

Figure 7: **Dimensional Change as a Function of Sintered Density and Sintering Temperature for FLN2-4405**

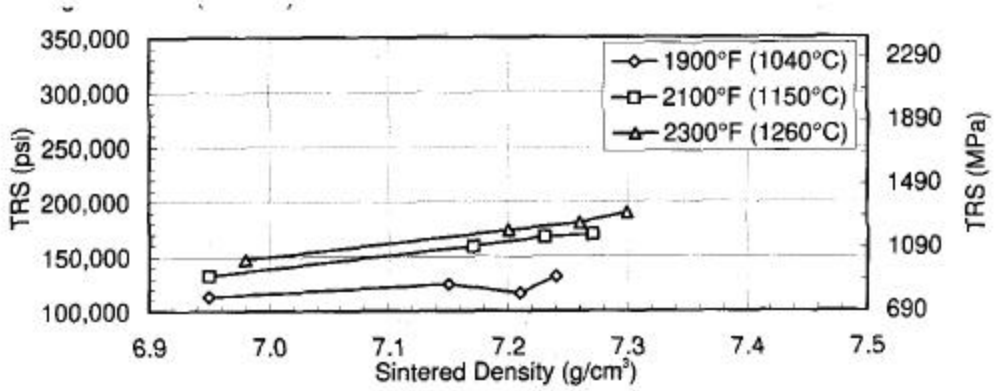

Figure 8: **Transverse Rupture Strength as a Function of Sintered Density and Sintering Temperature for FL-4405**

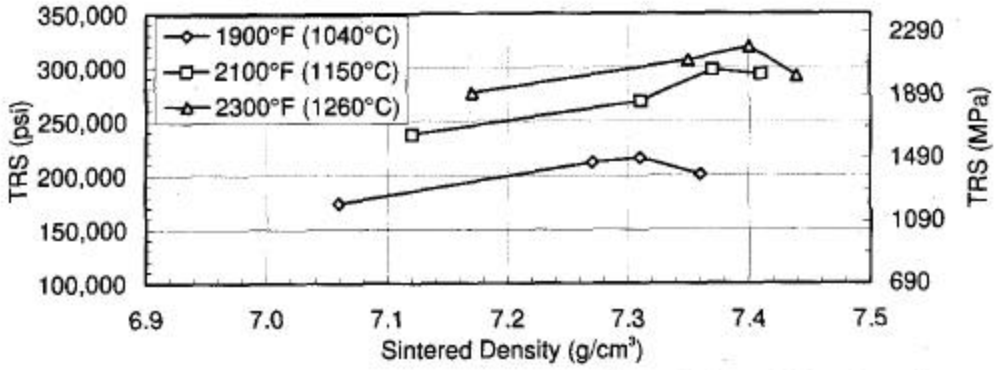

Figure 9: **Transverse Rupture Strength as a Function of Sintered Density and Sintering Temperature for FLN6-4405**

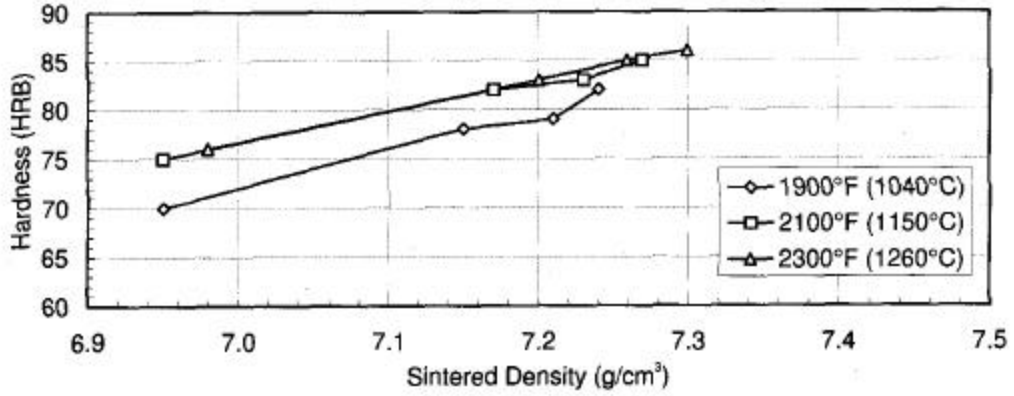

Figure 10: **Apparent Hardness as a Function of Sintered Density and Sintering Temperature for FL-4405**

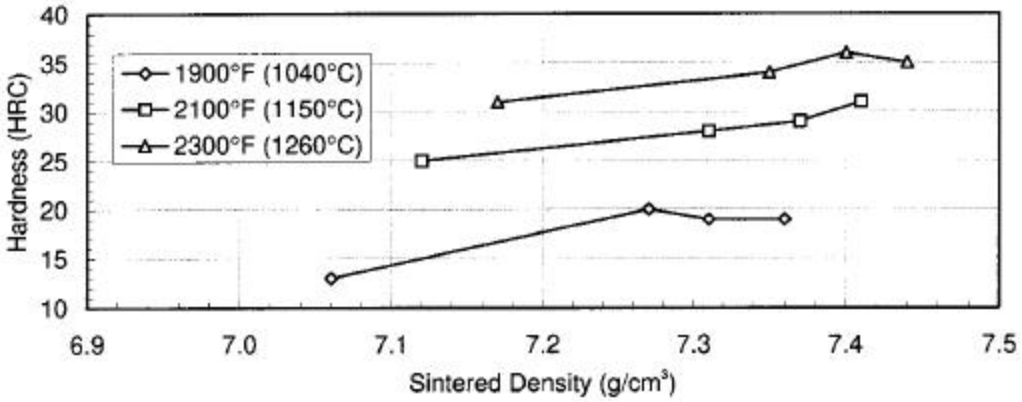

Figure 11: Apparent Hardness as a Function of Sintered Density and Sintering Temperature for FLN6-4405

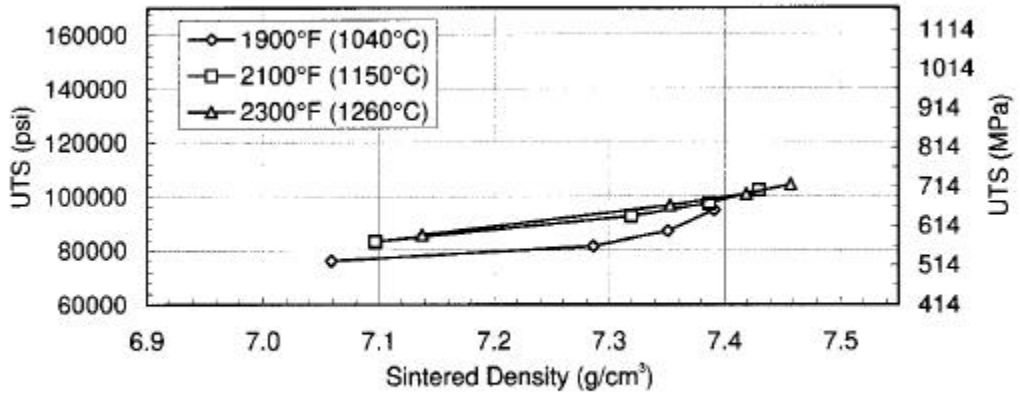

Figure 12: Ultimate Tensile Strength as a Function of Sintered Density and Sintering Temperature for FLN2-4405

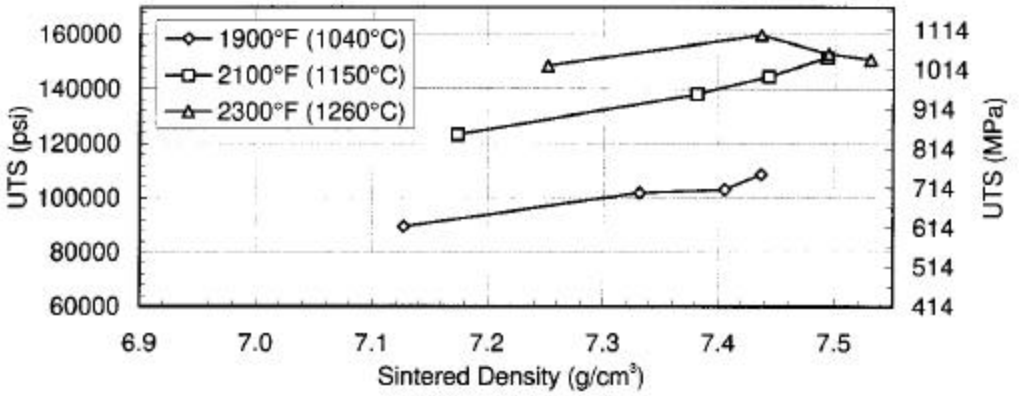

Figure 13: **Ultimate Tensile Strength as a Function of Sintered Density and Sintering Temperature for FLN6-4405**

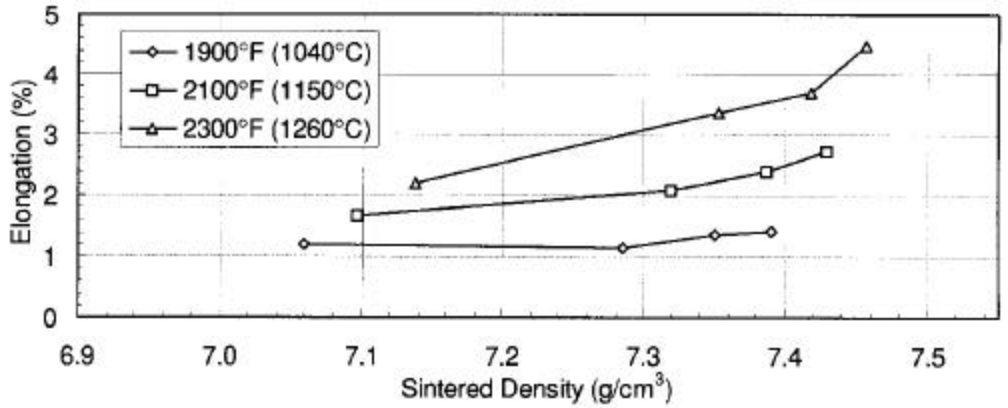

Figure 14: **Elongation as a Function of Sintered Density and Sintering Temperature for FLN2-4405**

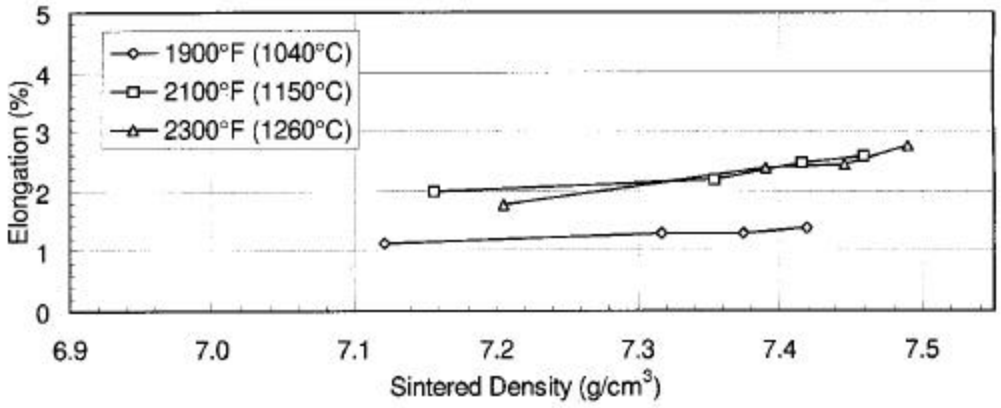

Figure 15: Elongation as a Function of Sintered Density and Sintering Temperature for FLN4-4405

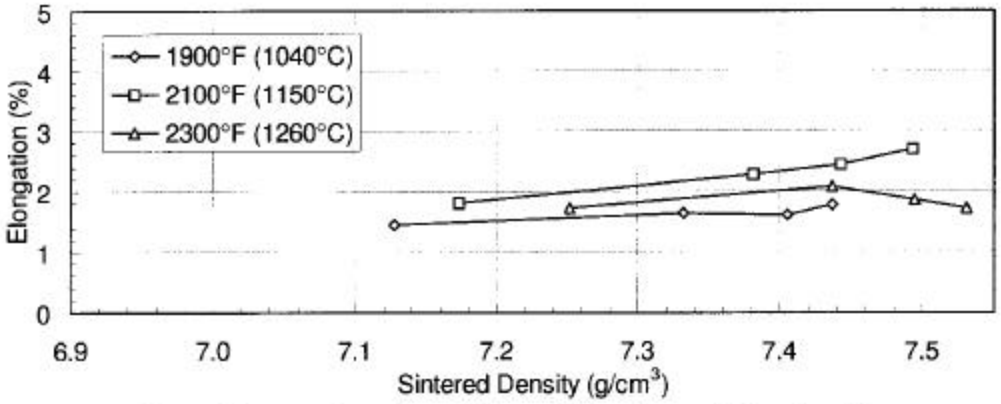

Figure 16: Elongation as a Function of Sintered Density and Sintering Temperature for FLN6-4405

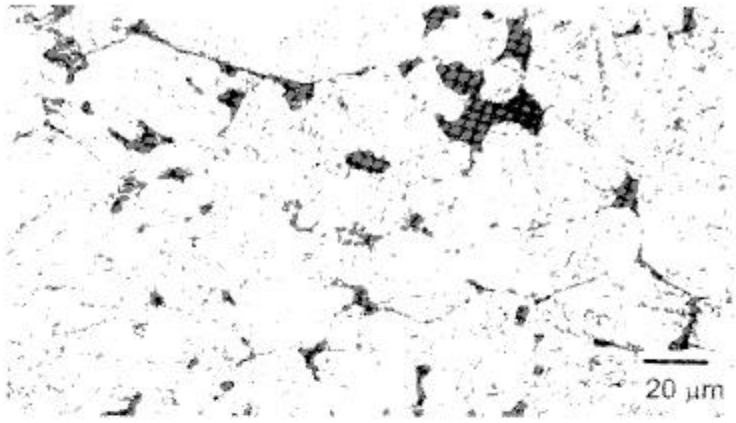

Figure 17: **Photomicrograph of FL-4405 at 1900°F(1040°C) (Original Magnification 500x)**

Figure 18: **Photomicrograph of FL-4405 at 2100°F(1150°C) (Original Magnification 500x)**

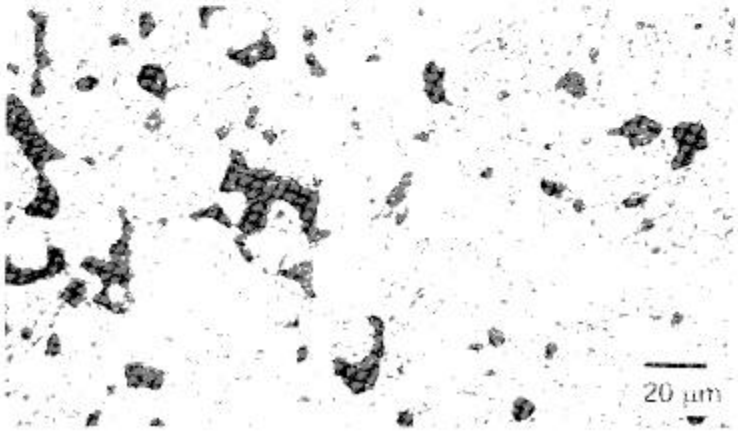

Figure 19: **Photomicrograph of FL-4405 at 2300°F(1260°C) (Original Magnification 500x)**

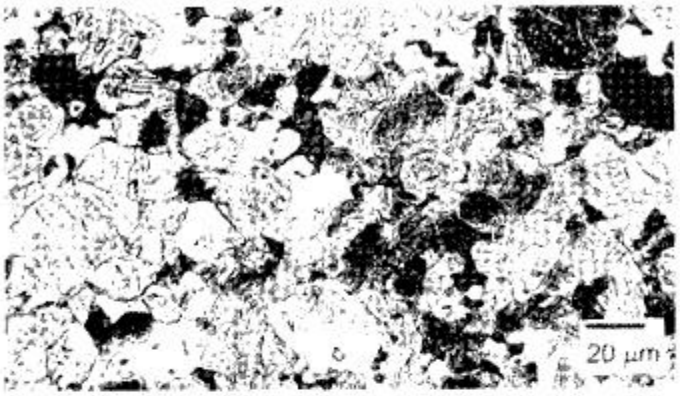

Figure 20: **Photomicrograph of FLN2-4405 at 1900°F(1040°C) (Original Magnification 500x)**

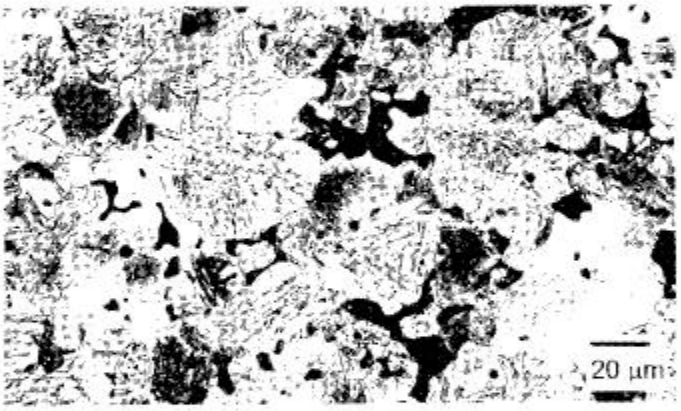

Figure 21: **Photomicrograph of FLN2-4405 at 2100°F(1150°C) (Original Magnification 500x)**

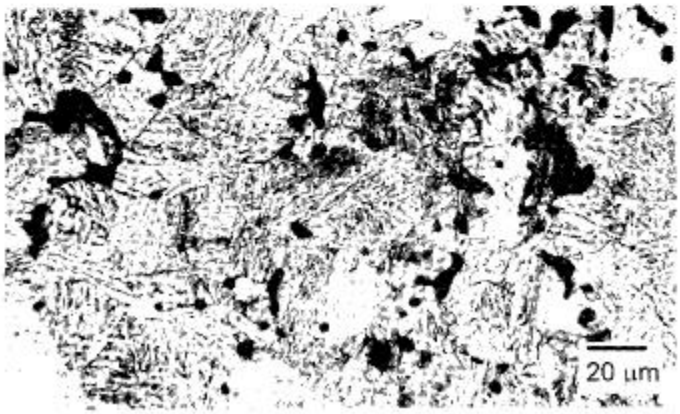

Figure 22: **Photomicrograph of FLN2-4405 at 2300°F(1260°C) (Original Magnification 500x)**

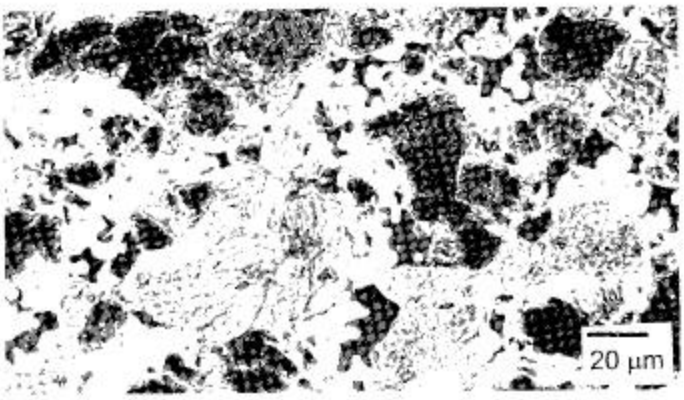

Figure 26: Photomicrograph of FLN6-4405 at 1900°F(1040°C) (Original Magnification 500x)

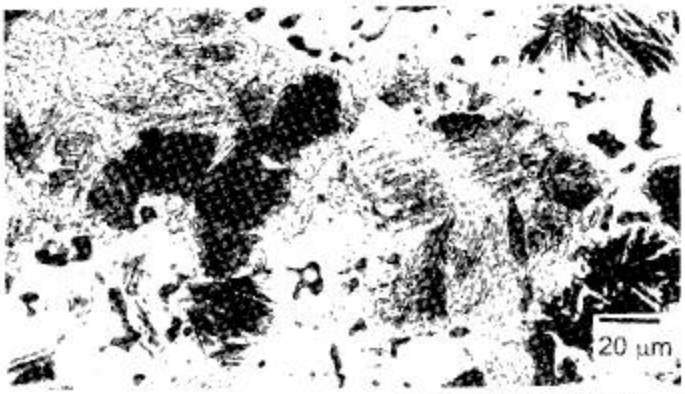

Figure 27: Photomicrograph of FLN6-4405 at 2100°F(1150°C) (Original Magnification 500x)

Figure 28: Photomicrograph of FLN6-4405 at 2300°F(1260°C) (Original Magnification 500x)